Directional Modulation from a Wrist-Wearable Compact Antenna

Abel Zandamela*, Nicola Marchetti*, Adam Narbudowicz*,
*CONNECT Centre, Trinity College Dublin, Dublin, Ireland
{zandamea, nicola.marchetti, narbudoa}@tcd.ie

***Abstract*—This work proposes compact multiport antennas for directional modulation (DM) on wrist-wearable devices to improve the secrecy and privacy of the transmitted data. The DM performance is investigated using the antenna in free-space and with a human forearm-phantom. The system achieves a low Bit Error Rate (BER) $< 10^{-1}$ with 44° beamwidth, in a unique steerable secure direction over the entire azimuth plane. Full-wave simulations including the phantom at $5\,\text{GHz}$ show realized gains of up to $4.26\,\text{dBi}$. The specific absorption rate is below the standard limits, with maximum values of $0.487\,\text{W/kg}$ and $1.42\,\text{W/kg}$ for the wrist-worn and next-to-mouth conditions, respectively.**

***Index Terms*—Wrist-wearable antennas, Internet of Things (IoT), Directional Modulation (DM), Compact IoT devices.**

I. Introduction

Directional Modulation (DM) is a keyless wireless physical-layer security technology. The method uses multiple-antennas to enable transmission of spatially scrambled constellation symbols along undesired eavesdropper directions, while preserving the original constellations in the pre-specified secure direction of the legitimate receiver [1], [2]. DM explores physical-layer properties to improve communication secrecy, instead of computationally expensive encryption standards in upper layers. This feature makes it a particularly good candidate for enhanced security in wireless transmissions from small Internet of Things (IoT) platforms. This is the case for wrist-wearable devices, as they are battery-operated with limited computational power [3], [4], which leads to inadequate encryption regime, raising privacy and security concerns of their connectivity [5]. Another issue with wrist-wearable devices is that the integrated antennas need to be compact to allow suitable packaging for wrist use. In addition, the design process needs to account for phenomena like efficiency deterioration, and pattern distortion due to the coupling with the human body [3], [4].

In this paper, we investigate for the first time in the open-literature, directional modulation from wrist-wearable devices. Although most DM implementations use antenna arrays [1], [2]; DM using compact antennas is investigated in [6], [7]. However, these implementations are either limited within ($0^\circ - 180^\circ$), have too high-profile for wrist-wearable devices, or the secrecy can be compromised by high side-lobe levels. In this work, the proposed antenna has 0.65λ diameter and 0.19λ height. The solution achieves unidirectional beamsteering over the entire horizontal plane. Therefore, the DM performance is investigated in the same plane, with the antenna in free-space and including the human forearm-phantom. In both cases a unique steerable secure transmission direction is realized. The system shows low Bit Error Rate (BER), with BER $< 10^{-1}$ of 44° beamwidths.

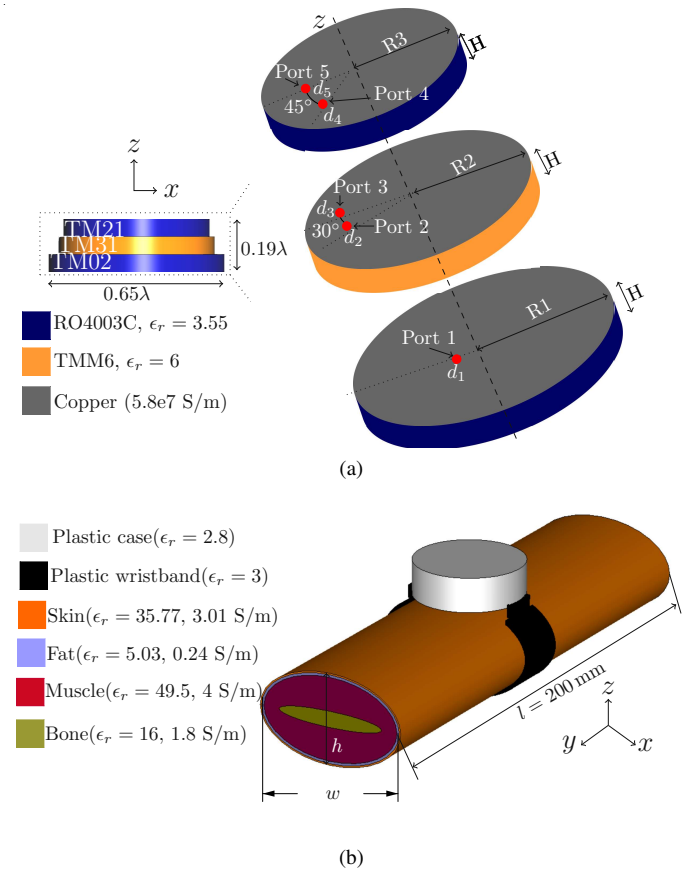

Fig. 1. Proposed system: (a) $xz-$plane and exploded perspective views (not drawn to scale) of the proposed antenna with corresponding radiating modes, antenna diameter, thickness and marked ports; (b) Final set-up including plastic case, plastic wristband and human forearm-phantom (with the antenna placed inside the plastic case).

II. System Design

A. Antenna Design

The proposed antenna is shown in Fig. 1(a). The antenna

incorporates three co-located dielectric loaded circular patches. Each patch is made of a substrate with H $=$ 3.81 mm thickness and a copper layer with 0.035 mm thickness. A total of five different orthogonal omnidirectional radiating modes are excited within the three patches. The top-patch excites two orthogonal TM_{21} modes, the middle-patch excites two orthogonal TM_{31} modes, and the bottom-patch excites the monopole-like TM_{02} mode.

The antenna is designed to operate at the center frequency of $f_0 = 5$ GHz. The top-patch (of radius R3 $= 16.2$ mm) is supported by the Rogers substrate RO4003C (relative permittivity $\epsilon_r = 3.55$ and loss tangent tan$\delta = 0.0027$). To excite the TM_{21} modes, the patch is fed using ports 5 and 4. Port 5 is located at $d_5(x, y) = (10, 0)$ mm; Port 4 is located at $d_4(x, y) = (7, 7)$ mm, oriented by 45° in respect to port 5. For antenna miniaturization, the patch exciting the higher order TM_{31} modes is supported by a substrate of higher relative permittivity [8] Rogers TMM6 ($\epsilon_r = 6$ and tan$\delta = 0.0023$). Port 3 and port 2 are located in the middle-patch (radius R2 $= 17.3$ mm) at $d_3(x, y) = (9.5, 0)$ mm, and $d_2(x, y) = (8.2, 4.8)$ mm, respectively. The bottom-patch (radius R1 $= 19.5$ mm) uses the RO4003C substrate, and is fed by port 1 located at $d_1(x, y) = (5, 0)$ mm. The antenna total dimensions are: 39 mm × 39 mm × 11.6 mm or $0.65\lambda \times 0.65\lambda \times 0.19\lambda$, where λ is the wavelength at $f_0 = 5$ GHz.

B. Forearm-Phantom

To study the impact of the human forearm on the antenna performance, a phantom is integrated and is shown in Fig. 1(b). The phantom has a total length of $l = 200$ mm, width $w = 60$ mm, and thickness $h = 36$ mm. It is comprised by four layers: skin, fat, muscle and bone. The proportions of the volume for each layer are defined following the computed tomography results discussed in [9], and are outlined in Table I. The dielectric properties of each layer at $f_0 = 5$ GHz are obtained from [10], and are also detailed in Table I.

The antenna shown in Fig. 1(a) is placed at the center of the forearm-phantom (at $l = 100$ mm), with the groundplane of the bottom-patch in direct contact with the skin layer. The case of the wrist-worn device is simulated by a plastic case of $\epsilon_r = 2.8$ and tan$\delta = 0.01$. A spacing of 1 mm is introduced between the antenna and the plastic case. The wall thickness of the plastic case is 1 mm, and the case total diameter and height are 42.98 mm and 13.57 mm, respectively. A plastic wristband ($\epsilon_r = 3$) of width $= 20$ mm and thickness $= 3$ mm is attached at two opposite edges of the plastic case, surrounding the skin-layer of the phantom.

TABLE I
DIELECTRIC PROPERTIES (AT $f_0 = 5$ GHz) AND VOLUME PROPORTIONS OF THE INVESTIGATED FOREARM PHANTOM [9], [10].

Layer	ϵ_r	Conductivity (σ) S/m	Volume (%)
Skin	35.77	3.06	Skin + Fat =
Fat	5.02	0.24	15
Muscle	49.54	4.04	72.1
Bone	16.05	1.81	12.9

TABLE II
TOTAL EFFICIENCY AT $f_0 = 5$ GHz.

Total Efficiency	Antenna Ports				
	Port 1	Port 2	Port 3	Port 4	Port 5
Free-space	91%	49%	49%	87%	87%
Including Phantom	52%	37%	36%	67%	70%

III. ANTENNA PERFORMANCE

The proposed system is simulated using the finite-integration technique in CST Studio Suite. The antenna was analysed in free-space and including the forearm-phantom. The S-parameters in free-space are shown in Fig. 2(a), and the results with the forearm-phantom are shown in Fig. 2(b). The isolation is better than 17 dB with impedance bandwidth of 18.5 MHz in free-space; these values change to 13.7 dB and 23.5 MHz for the simulation including the phantom. The impact of the phantom on the antenna total efficiency is shown in Fig. 2(c) and detailed in Table II. The significant drop of

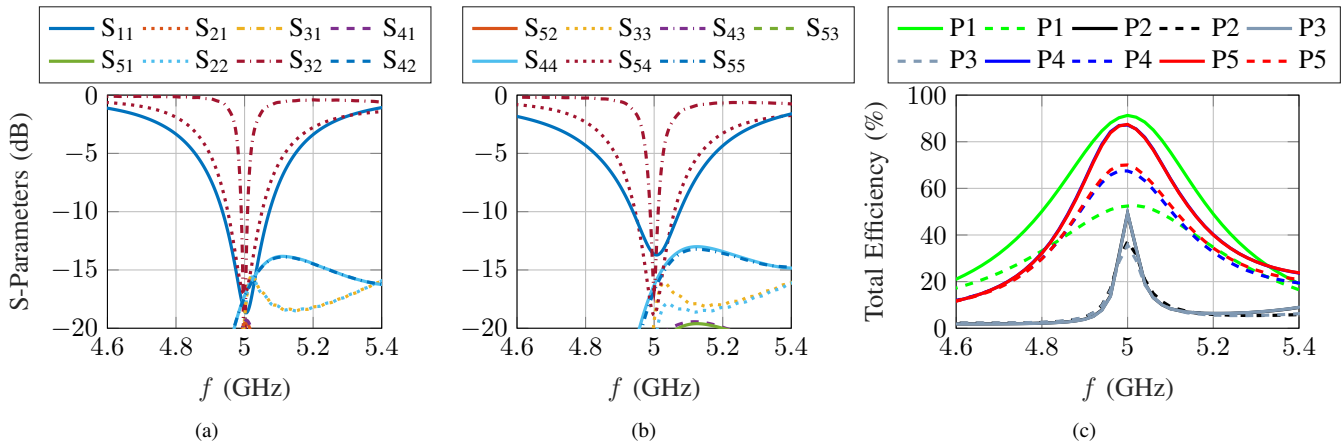

Fig. 2. Full-wave simulated results: (a) S-parameters of the proposed antenna in free-space and (b) with the forearm-phantom; (c) Total efficiency for each port in free-space (solid lines) and with forearm-phantom (dashed lines).

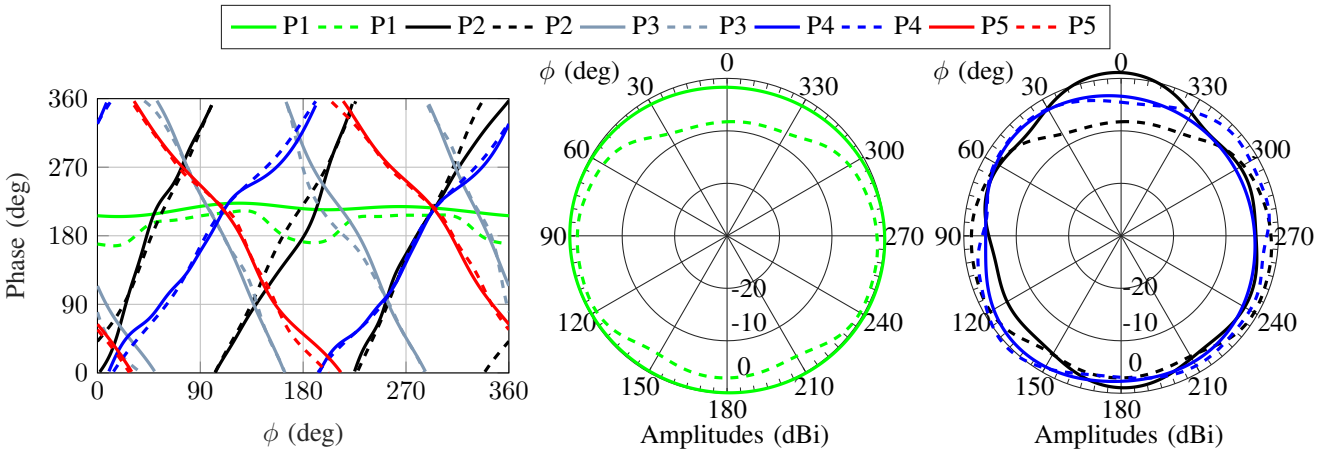

(a) (b) (c)

Fig. 3. Normalized simulated radiation patterns of the antenna in free-space (solid lines) and with the human forearm-phantom (dashed lines): (a) Phase of the radiation pattern of all antenna ports; (b) Amplitudes of port 1; (c) Amplitudes for ports 2 and 4;

the efficiency for port 1 can be explained by the bottom-patch close proximity to the phantom (the groundplane is placed in direct contact with the skin-layer). This results in increased energy and pattern tilt for the mode radiated by the bottom-patch. It is also worth mentioning that the TM_{02} mode is deliberately placed at the bottom because it is the most efficient radiator compared to other higher order modes [8]. Therefore additional losses still allow for efficiency $> 50\%$.

The antenna beamsteering is obtained by controlling the phase-shifts between the antenna feeding ports. The generated radiation patterns have their phase changing linearly in opposite directions along the azimuth-plane [Fig. 3(a)], twice for the TM_{21} modes, thrice for the TM_{31} modes and constant for the TM_{02} mode. The amplitudes of the patterns are shown in Fig. 3(b) for port 1 and Fig. 3(c) shows the amplitudes for port 2 (TM_{31}) and port 4 (TM_{21}). For brevity, the amplitudes of ports 3 and 5 are not shown as they also excite the aforementioned modes.

The achieved beamsteering is unidirectional over the entire azimuth plane as demonstrated in Fig. 4. The results show the performance when the main-beam is directed towards $0°, 30°, 60°, 90°, 270°, 300°$ and $330°$, for both cases (antenna in free-space and on the forearm-phantom). It can be seen that slight beam tilts are present when the phantom is included (of up to $9°$). They are more evident within the beams steered towards $(10° - 65°)$, $(120° - 170°)$, $(190° - 230°)$ and $(295° - 350°)$. This can be explained by the deeps (seen around the same intervals) on the phase of the radiation pattern of port 1 [Fig. 3(a)] and on the amplitudes deeps seen in [Fig. 3(b)] when the phantom effects are included. The phase of the radiation pattern and the amplitudes for the phantom-case are less uniform compared to the simulation when the antenna is operating in free-space; Consequently beam tilts effect on the phantom patterns are observed. However, a simple procedure to eliminate those can be the use of a phase-correcting parameter in the beamsteering formula.

From Fig. 4 it can also be seen that the pattern is not tilted when the beam is steered towards $0°$. This is because the main beam is exactly at the center of the phantom [$x = w/2$, see Fig. 1(b)], and the beam tilts are symmetrical (equal from both $-x$ and $+x$) directions. While this phenomenon do not impact the beamsteering, however, a drop of $2.86\,\mathrm{dB}$ on realized gain is observed at $0°$; from $4.15\,\mathrm{dBi}$ in free-space to $1.29\,\mathrm{dBi}$. This is due to the high energy absorption by the phantom at the center ($x = w/2$). The above is also true for $180°$ within $[90° - 270°]$. For $90°$ and $270°$ directions, the beamsteering including the phantom shows minimal tilts and negligible additional losses. This is because the steered beams lie in the orthogonal plane (xz), and hence are less exposed to the phantom effects. The gain is also not impacted and is

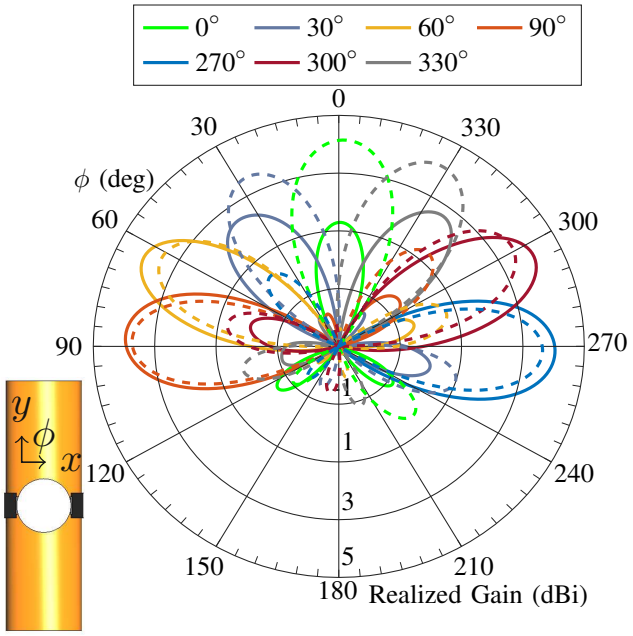

Fig. 4. Beamsteering performance of the antenna in free-space (dashed lines) and with the human forearm-phantom (solid lines).

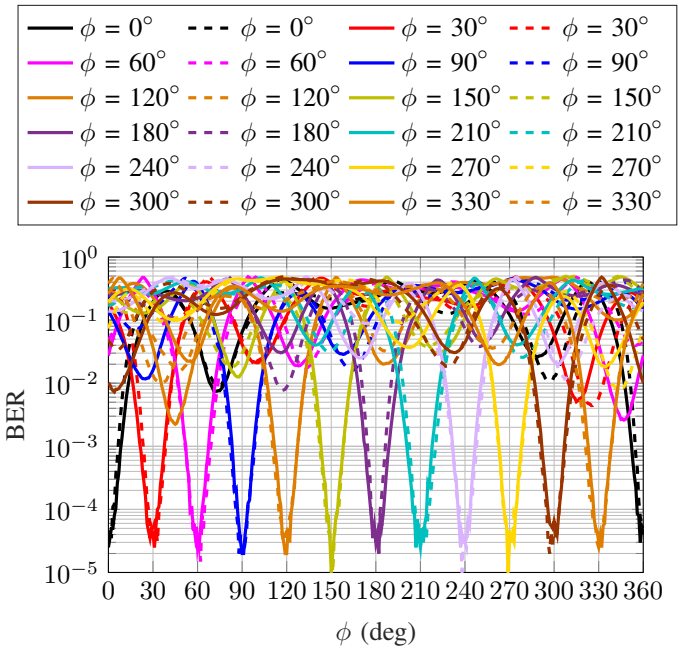

Fig. 5. BER calculations for 12 different beams separated by 30°, using SNR = 12 dB with (solid-lines) and without (dashed lines) phantom.

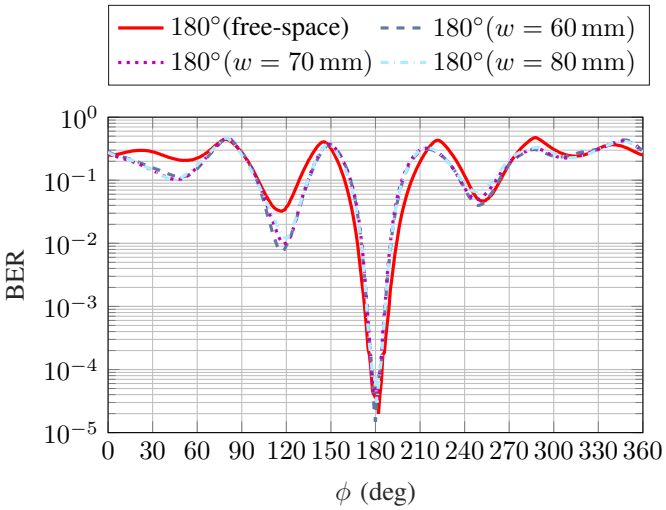

Fig. 6. BER calculations for $\phi_A = 180°$, using SNR = 12 dB for the antenna in free-space and with different widths of the human forearm-phantom.

up to 4.26 dBi.

IV. Directional Modulation

The proposed antenna realizes unidirectional beamsteering in the azimuth plane (Fig. 4), therefore the Directional Modulation (DM) is investigated in the same plane. Assuming that the receiver is located at a secure ϕ_A direction, the DM is realized by exciting each port of the antenna, and the transmitted signals are defined as [6]

$$s_{tn}(\phi_A) = \frac{\vec{m}}{P_n(\phi_A)} \tag{1}$$

where ϕ_A is the direction of the legitimate receiver, P_n is the complex radiation pattern generated by the antenna n^{th} port (with $n = 1...N$, where N is the total number of ports in the antenna), $\vec{m}$ is a complex modulation vector (including the artificially generated noise to spatially scramble the constellations in the eavesdropper directions, with the amplitude of the noise being equal to the amplitude of the signal).

To demonstrate the DM performance of the antenna, without loss of generality, we will assume the use of Quadrature Phase Shift Keying (QPSK). The DM performance metric used in this work is Bit Error Rate (BER), which is calculated for various directions along the azimuth plane using a data stream with 10^5 transmitted symbols. The required complex radiation patterns for each port (P_n) are extracted from CST Studio Suite and the DM calculations are performed using MATLAB. Furthermore, a 12 dB Signal-to-Noise Ratio (SNR) of Additive White Gaussian Noise (AWGN) is added in the receiver. The noise is assumed to be independent at each location.

Fig. 5 shows the BER of the antenna in free-space and including the phantom effects for width $w = 60$ mm. The results are shown for 12 different directions to cover the entire azimuth plane. It can be seen that the directionally modulated transmission can be steered towards any ϕ_A direction over the azimuth plane without leakage into undesired angles. Fig. 6 shows the BER calculations for the desired secure direction $\phi_A = 180°$ with the antenna in free-space and using different widths of the phantom. The beamwidth for BER $< 10^{-1}$ around the secure direction is within $44°[160° - 204°]$ in all the four cases. Overall, these results demonstrate that the steerable secure transmission direction is little impacted when the phantom is included.

To further illustrate the DM performance of the proposed system, Fig. 7 shows four exemplary QPSK constellations generated using the antenna in free-space and with the largest investigated width ($w = 80$ mm). The different transmitted symbols are shown in different colors. Fig. 7(a) and (c) show the constellations for the secure direction $\phi_A = 180°$. It is observed that for this direction a clear QPSK constellation is obtained, with each of the four clusters being comprised only by the same within-cluster transmitted symbols. Contrastly, for the constellations shown in the undesired direction $\phi = 150°$ [Fig. 7(b) and (d)], the symbols are scrambled and difficult to distinguish. Consequently, in the directions other than the legitimate receiver $\phi_A = 180°$, it is challenging for the eavesdropper receiver to correctly separate the transmitted symbols. This is expected to improve the secrecy and privacy of wrist-wearable devices transmitted data.

V. Electromagnetic (EM) Field Exposure

To investigate the levels of the EM field exposure of the proposed antenna, the specific absorption rate (SAR) is computed following the guidelines published by the Federal Communication Commission (FCC) [12]. The SAR is evaluated under two conditions: wrist-worn and next-to-mouth conditions (as some

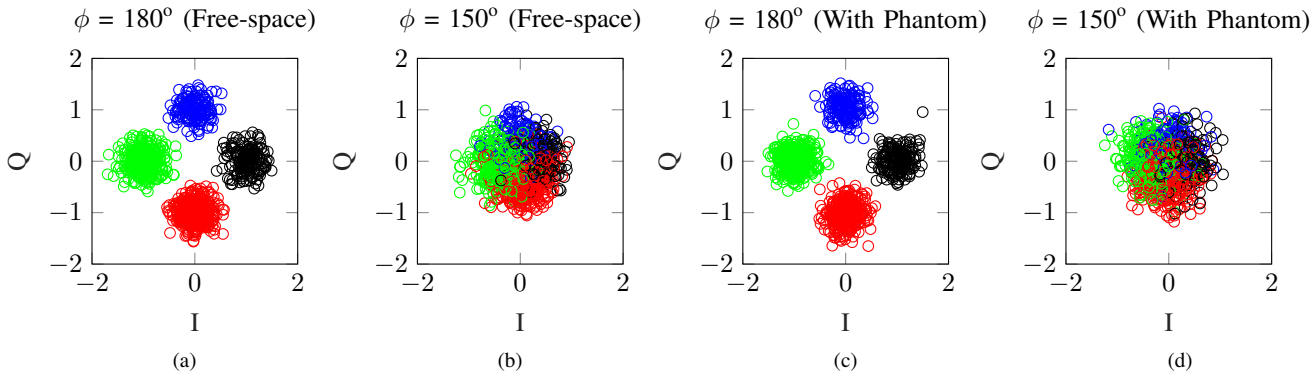

Fig. 7. Color coded QPSK constellations: ■ '00' ■ '01' ■ '11' ■ '10'; For secure $\phi = 180°$ and undesired $\phi = 150°$ directions.

devices may support voice-over communications). To quantify the SAR in the above conditions, the FCC recommends using a flat phantom that is filled with hand and head tissue-equivalent medium. In the wrist-worn case, the back of the device should be positioned in direct contact with the flat phantom, without any spacing [Fig. 8(a)]. In the next-to-mouth condition, the front of the device should be positioned at $10\,\mathrm{mm}$ from the flat phantom [Fig. 8(b)].

Table III shows the SAR values of the wrist-wearable device. For portable devices the input power is typically in the order of mW levels, and for $100\,\mathrm{mW}$ the SAR values are below the FCC limits, which are $(4\,\mathrm{W/kg})$ for the wrist-worn condition, and $(1.6\,\mathrm{W/kg})$ for next-to-mouth condition.

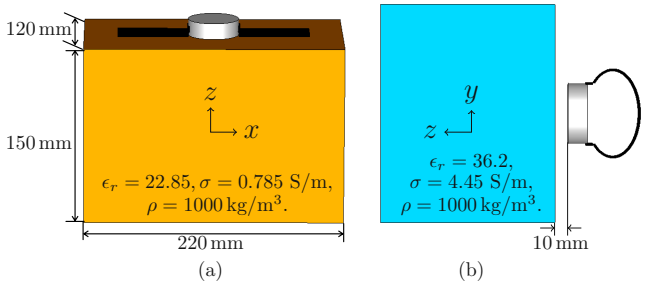

Fig. 8. CST Studio Suite set-ups for SAR computation at $f_0 = 5\,\mathrm{GHz}$: (a) wrist-worn and (b) next-to-mouth conditions.

TABLE III
SAR [W/KG] AT $f_0 = 5\,\mathrm{GHz}$ FOR $100\,\mathrm{mW}$ INPUT POWER.

SAR (W/kg)	Antenna Ports (100 mW)				
	Port 1	Port 2	Port 3	Port 4	Port 5
Wrist-worn average in 10g	0.34	0.49	0.4	0.24	0.18
Next-to-mouth average in 1g	0.57	0.33	0.31	1.42	1.41

VI. Conclusion

This work investigated for the first-time in the open-literature directional modulation from a compact wrist-wearable antenna (of size $0.65\lambda \times 0.65\lambda \times 0.19\lambda$). Full-wave simulations including a forearm-phantom demonstrated the system capability of data transmission in a unique steerable secure direction across the full azimuth-plane. The beamwidth with BER $< 10^{-1}$ is $44°$ and the realized gain deterioration due to the phantom presence is less than $2.86\,\mathrm{dB}$ across the entire plane. Overall, it demonstrates the ability to use additional privacy offered by directional modulation within wearable medical devices.

Acknowledgment

This publication has emanated from research conducted with the financial support of Science Foundation Ireland under Grant number 18/SIRG/5612.

References

[1] M. P. Daly and J. T. Bernhard, "Directional Modulation Technique for Phased Arrays", *IEEE Trans. Antennas Propag.*, vol. 57, no. 9, 2009.
[2] Y. Ding and V. F. Fusco, "A Vector Approach for the Analysis and Synthesis of Directional Modulation Transmitters", *IEEE Trans. Antennas Propag.*, vol. 62, no. 1, pp. 361-70, Jan. 2014.
[3] S. Yan, et al., "Wearable Dual-Band Magneto-Electric Dipole Antenna for WBAN/WLAN Applications", *IEEE Trans. Antennas Propag.*, vol. 63, no. 9, Sept. 2015.
[4] D. Wu and S. W. Cheung, "A Cavity-Backed Annular Slot Antenna With High Efficiency for Smartwatches With Metallic Housing", *IEEE Trans. Antennas Propag.*, vol. 65, no. 7, pp. 3756-3761, July 2017
[5] S. Banerjee, T. Hemphill, and P. Longstreet, "Wearable devices and healthcare: data sharing and privacy," *Information Society*, vol. 34, no. 2, pp. 1–9, 2017.
[6] A. Narbudowicz, M. J. Ammann and D. Heberling, "Directional Modulation for Compact Devices", *IEEE Antennas Wirel. Propag. Lett.*, vol. 16, pp. 2094-2097, 2017
[7] J. Parron, et al., "Multiport Compact Stacked Patch Antenna With 360° Beam Steering for Generating Dynamic Directional Modulation", *IEEE Trans. Antennas Propag.*, vol. 69, no. 2, pp. 1162-1167, Feb. 2021
[8] A. Zandamela, et al., "On the Efficiency of Miniaturized 360° Beam-Scanning Antenna", *13th EuCAP Conference*, Poland, 2019.
[9] R. J. Maughan, S. J. Watson, and J. Weir, "The relative proportions of fat, muscle and bone in the normal human forearm as determined by computed tomography", *Clin Sci (Lond)*, Jun. 1984.
[10] C. Gabriel, "Compilation of the dielectric properties of body tissues at RF and microwave frequencies", Report N.AL/OE-TR-, Brooks Air Force Base, Texas (USA), June 1996, http://niremf.ifac.cnr.it/tissprop/.
[11] A. Zandamela, et al., "Digital pattern synthesis with a compact MIMO antenna of half-wavelength diameter," *AEÜ – Int. J. Electron. Commun.*, vol. 135, Jun. 2021.
[12] 447498 D01 General RF Exposure Guidance v06, RF Exposure Procedures and Equipment Authorization Policies for Mobile and Portable Devices, Federal Commun. Commission Office Eng. Technol. Lab. Division, Washington, DC, USA, Oct. 2015.